# Oxide dispersion strengthened bond coats with higher alumina content: Oxidation resistance and influence on thermal barrier coating lifetime

Authors: C.Vorkötter<sup>A</sup>; S.P.Hagen<sup>B</sup>;G.Pintsuk<sup>C</sup>; D.E.Mack<sup>A</sup>; S. Virtanen<sup>B</sup>; O.Guillon<sup>A,D</sup>; R.Vaßen<sup>A</sup>
Affiliations:

<sup>A</sup> Forschungszentrum Jülich GmbH, Institute of Energy and Climate Research, Materials Synthesis and Processing (IEK-1), 52425 Jülich, Germany E-mail: c.vorkoetter@fz-juelich.de – Tel. +49 2461 61-96735;

Sebastian.p.hagen@fau.de;
g.pintsuk@fz-juelich.de;
d.e.mack@fz-juelich.de;
virtanen@ww.uni-erlangen.de;
o.guillon@fz-juelich.de;
r.vassen@fz-juelich.de

<sup>B</sup> Friedrich-Alexander Universität Erlangen-Nürnberg, Chair for Surface Science and Corrosion, 91058 Erlangen, Germany

<sup>C</sup> Forschungszentrum Jülich GmbH, Institute of Energy and Climate Research, Plasma Physics, (IEK-4), 52425 Jülich, Germany

<sup>D</sup> Jülich Aachen Research Alliance, JARA-Energy

Corresponding author: Christoph Vorkötter

Key words: oxide dispersion strengthened, thermal barrier coating, beta depletion, Y-diffusion, thermal spray

### **Abstract:**

The oxidation resistance of the bond coat in thermal barrier coating systems has significant influence on thermal cycling performance of the protective coating.

In this study the influence of varying the alumina content of plasma sprayed oxide dispersion strengthened bond coats with CoNiCrAlY matrix material on the oxidation resistance was analyzed by thermogravimetric analysis, SEM and TEM.

Yttrium ions at the alumina scale grain boundaries and the grain size in the scale appear as major factors influencing oxidation properties.

The ODS material with 2, 10 and 30 wt.% alumina content was applied in TBC systems as an additional thin bond coat. The thermal cycling performance of those advanced TBC systems, in burner rig tests, was evaluated in respect to the ODS material properties. Thermal cycling

behaviour is in good correlation to the isothermal oxidation resistance. All results indicate that TBC systems with 10 % alumina content in the ODS bond coat have a superior thermal cycling performance, as compared to ODS bond coats with lower or higher alumina.

### Introduction

Thermal barrier coatings (TBCs) are commonly used to protect gas turbine engine components, such as turbine blades, from damage caused by high temperatures and reactive environments. To reach optimal protection function of the TBC system two different material classes, namely ceramics and metal alloys, need to be combined. TBCs typically consist of a ceramic top coat (common material: Yttria Stabilized Zirconia - YSZ) on top of a metallic bond coat (mostly MCrAlY – M=Co, Ni). If the gas turbine is cooled from the inside, the top coat provides a thermal gradient between the TBC surface and the gas turbine component, due to low thermal conductivity of ceramics. The metallic bond coat ensures oxidation protection of the gas turbine component material and enhances top coat adhesion.

Thermal mismatch between the ceramic top coat and the substrate material is a main factor leading to stresses at the metal ceramic interface and within the top coat during thermal cycling, which finally leads to crack propagation and failure of the coating. If the TBC system is assumed stress free at room temperature, the top coat is under tensile stress after heating the TBC, due to the higher thermal expansion coefficient of the substrate. At high temperatures, stress relaxation within the top coat leads to compressive stresses in the top coat after subsequent cooling of the TBC system. The top coat under compressive stress stores energy which provides crack propagation and finally causes failure of the coating.

On a smaller length scale, the mismatch of the bond coat and the top coat leads to additional tensile stresses at the tip of a wavy interface between top coat and bond coat after cooling down

the TBC system. Thus a reduced mismatch has a positive influence on the stress field at the bond coat top coat interface, which leads to a prolonged TBC lifetime [1–3].

The thermally grown oxide layer (TGO), between the ceramic top coat and the metallic bond coat, has a low thermal expansion coefficient and affects stress inversion and tensile stresses at the valleys of the wavy interface [1], which can lead to crack linking and finally failure of the coating. Therefore, both the oxidation resistance and the thermal expansion coefficient of the bond coat affect the stress field in the wavy interface and hence play a major role in the thermal cycling performance of the TBC system.

The addition of an oxide phase in the bond coat material (oxide dispersion strengthened - ODS - materials) leads to increased scale adherence and an increased oxidation resistance [4,5].

The increase in oxidation resistance of oxide dispersion strengthened material can be related to the formation of a homogeneous closed alumina TGO, with a proper amount of Y at the grain boundaries, provided by the alloy, affecting the oxygen diffusion through the scale [4,6–9].

The effects of reactive element (RE) doping with for instance Y in the alloy, or in this case the bond coat material, is summarized as the "reactive element effect" [10,11]. The exact mechanism of the reactive element effect is still under debate, however, the effect is based on a decrease of the cationic and anionic (O) outward and inward flux during oxidation, due to reactive element enrichment at the TGO grain boundaries. Driven by the gradient of the oxygen potential, yttrium is known to segregate through the alumina scale towards the surface, taking mainly the scale grain boundaries as the easiest path for diffusion [7,12]. As described by previous studies, yttrium as a reactive element in the bond coat furthermore influences the role of S on the alumina scale and by that increases the scale adherence, which can be related to improved TBC performance [6,11,13].

However, the amount of Y is critical and a reactive element overdoping can even lead to an early TBC failure due to Y pegs in the TGO inducing additional stresses [14–16]. By the use of ODS the risk of overdoping can be suppressed by the alumina particles. The latter are found to interact with Y and are thus preventing an excessive incorporation of Y causing aluminates to nucleate within the TGO [5,9,17].

In a TBC system, oxide dispersion strengthened bond coats with 2 % alumina content reveal a high oxidation resistance [18], leading to an increased thermal cycling performance, even by use as a thin additional layer (flash coat) on the standard bond coat [5,17].

In this study, the thermal mismatch at the bond coat top coat interface of the TBC is reduced, compared to the standard bond coat, by the use of ODS material as an additional thin flash coat. The influence of different ODS contents (non-ODS 0 %, 2, 10 and 30 wt. %) is investigated. Through the high alumina content the bond coat coefficient of thermal extension (CTE) is reduced from 16.6 10<sup>-6</sup> 1/K down to 12.7 10<sup>-6</sup> 1/K.

As a second effect, the oxidation resistance of the ODS material is significantly influenced by increased alumina content. TGA analysis and TEM images of the oxide scale show Y at the alumina scale grain boundaries of 2, 10 and 30 % alumina ODS material. 10 % alumina ODS material reveals comparable good oxidation resistance to 2 % ODS. Analysis of ODS bond coat TBCs, thermally cycled under conditions close to operational, shows the major influence of the bond coat properties on the TBC performance and failure mechanism. The performance of 10 % ODS TBCs is superior to the previously reported TBC systems [5,19] due to high oxidation resistance and low ODS bond coat thermal expansion coefficient.

# **Experimental procedure**

Three oxide dispersion strengthened material powders were produced by mechanical alloying. The alumina content of the sprayed material ranged from 0, 2, 10 up to 30 wt. % to elucidate the influence of alumina content on oxidation resistance and on the TBC performance. For this purpose the powders were thermally sprayed as thick (1 mm) free standing coatings or as a thin (50 µm) additional bond coat on a conventional bond coat in TBC systems with a Yttria Stabilized Zirconia (YSZ) top coat.

## Powder production

Oxide dispersion strengthened powders were produced in several milling runs using a high energy milling facility (Attritor Simoloyer CM01, ZoZ GmbH, Wenden, Germany) with a one litre steel milling chamber, 5 mm diameter steel balls and a powder to ball ratio of 1:10. Each milling run was conducted for a 120 g powder mixture of CoNiCrAlY (Amdry 995 Oerlicon Metco, Wholen, Switzerland), alumina (Martoxid MR70, Martinswerk, Bergheim, Germany) and in case of 2 % alumina addition furthermore a process control agent. A milling procedure took 4-6 h whereas the milling speed was cyclically varied. One milling speed cycle was 1 min at 500 rpm and 4 min at 870 rpm. In order to compensate the different powder properties milling parameters were slightly varied. Thus, in case of 2 % alumina powder mixture 0.5 wt. % stearic acid was added to the powder mixture as a process control agent in order to diminish cold welding during milling (6 h). Stearic acid addition and milling speed cycling assure a good embedding of the alumina in the base material [20]. For 10 and 30 % alumina, stearic acid addition was not necessary and the milling time could be reduced to 4 h. To ensure a good alumina embedding at 30 % alumina powder the milling speed/mixing speed was increased to 1600/800 rpm. Milling parameters are presented in Table 1.

Spraying thick coatings and several flash coats requires a rather large amount of powder. Therefore the sieved 30 % ODS powder batch was enlarged by some ODS powder with the same powder microstructure, but slightly different milling production parameters.

Table 1 Oxide dispersion strengthened powder milling parameters for 120 g powder mixture per milling run

Powder	Milling	Milling	Process	Mixing
alumina	speed	time	control	speed
content	[rpm]	[h]	agent	[rpm]
[wt. %]				
2 %	870	6	0.5 wt .%	500
10 %	870	4	-	500
30 %	1600	4	-	800
0 %	no milling	-	-	-

To increase powder quality, 2 % alumina containing bond coat powders that were used for the TBC samples were sieved to 36-56 μm. However, to increase the efficiency of powder production, the higher fraction of 20-56 μm was used for all other samples. This was necessary to ensure a higher powder gain per milling run, especially for the thick free standing ODS samples. Chemical compositions were measured by inductive coupled plasma optical emission spectroscopy and combustion analysis. Size distributions were determined by laser diffraction with a Horiba LA-950 V2 (Horiba Ltd, Kyoto, Japan). Data are given in Table 2.

**Table 2** Chemical compositions in weight percent taken from [17,21] for ERBO1 and Amdry995 and from chemical analysis for the ODS powder. Also size distributions are shown, for 2 % ODS the values for the 20-56  $\mu$ m sieving fraction (for 36-56  $\mu$ m in brackets) are provided.

Material	Ni	Со	Cr	w	Re	Мо	Al	Ti	Ta	Fe	С	Y	О	D <sub>10</sub>	D <sub>50</sub>	D <sub>90</sub>
Widterial IVI	Co	CI	VV	RC	IVIO	0 Ai	11	1 a	rc		1	O	[µm]	[µm]	[µm]	
ERBO1	Bal	9	6.5	6	3	0.6	5.6	1	6.5	-	0.01		-	-	-	-
Amdry 995	34	Bal	21.3	-	-	-	8.39	-	-	-	-	0.42	-	21	32	49
2 % ODS	31.5	37.7	20.8	0.04	-	-	8.7	-	0.01	0.28	0.32	0.46	1.13	21 (32)	34 (48)	52 (72)
10 % ODS	29.8	35.6	19.7	0.02	-	-	12.7	ı	0.01	0.12	0.03	0.42	4.62	25	37	53
30 % ODS	22.4	27.2	14.9	0.07	-	-	20.1	-	0.02	1.56	0.05	0.28	13.04	12	29	49

## Spray process

Thick TGA samples were produced by vacuum plasma spraying (F4 gun Oerlicon Metco, Wholen, Switzerland) the four different bond coat powders to achieve a low amount of pores and mixed oxides in the coating using the 20-56 µm ODS-powder fraction.

1 mm thick bond coats were sprayed on 35x30 mm grid blasted steel blocks. From those samples (31x25x1 mm) freestanding ODS coatings were detached by spark erosion. Two thermogravimetric analysis (TGA) samples (13x20x1 mm) were produced for each alumina concentration. Spray parameters see

Table 3.

Complete TBC samples were produced by spraying a thin (50 µm) ODS bond coat on top of a standard bond coat (120 µm) or by using a single layered standard bond coat (160 µm). Bond coated samples were annealed for 4 h at 1140°C and 16 h at 870°C to increase the bond coat adhesion. The bond coat roughness was measured by a Cyberscan CT350 with a confocal white light sensor CHR1000 (CyberTECHNOLOGIES GmbH, Ingolstadt, Germany).

A Multicoat facility (Oerlikon Metco, Wohlen, Switzerland) with a three-cathode TriplexPro<sub>TM</sub> 210 atmospheric plasma spray gun was used to apply the about 500 µm thick YSZ (powder 204NS Oerlicon Metco, Wholen Switzerland) top coat to all TBC thermal cycling samples. Spraying parameters are presented in

Table 3. For 2 % ODS the 36-56 μm powder fraction was used.

## Isothermal oxidation

One of the two TGA samples was kept as produced with one rough side and an opposing spark eroded side. These two-sided samples are referred to as "as-sprayed" in the following. Both surfaces of the other kind of TGA samples were polished to 1 µm surface finish and are referred to as "polished". Sample preparation prior to oxidation was finished by a degreasing step in an

ultrasonic bath by acetone (3 min) and subsequent ethanol (3 min). Isothermal and time resolved thermogravimetric analysis using a SETSYS Evolution 1650 TGA (SETARAM Instrumentation, Caluire, France) were carried out at 1100°C for 70 h in an atmosphere containing 20 % oxygen and 80 % argon at normal pressure to provide comparability to previous studies [18].

While heating was performed in the before mentioned atmosphere, the cooling process was conducted in pure argon. Heating and cooling was performed with a rate of 25 K/min. Gas flow rates were set to 20 ml/min, which equals a laminar gas velocity of about 7.86 cm/min. For recording the mass gains, zeroing of the scale was performed at room temperature, thus mass changes evolving during heating of the sample are considered.

For high quality cross sections of the oxidized TGA, Ni-plating was applied prior to metallurgical preparation. For Ni-plating, first a thin Au-layer was applied by sputtering. Then galvanostatic electroplating was performed with Ni out of a NiSO<sub>4</sub> based solution with a current density of 15 mA/cm<sup>2</sup> for 30 min. Afterwards samples were halved by a water-cooled saw with very low feed rate. For the cross section preparation an ion milling system (IM4000 from Hitachi) was used. Particular attention was paid to allocate the ion milling cut at least 5 mm away of the sample's margin to prevent edge effects.

For TEM investigation of the polished TGA samples a lamella (4x10x1 µm) was cut out of oxidized samples by focused Ion beam at 30 kV (Helios G4 CX, FEI). TEM images were taken at MPI Düsseldorf equipped with a Super X-EDX detector in STEM mode (Mode for high resolution: high angle annular dark field - HAADF) at 300 kV for the element mapping (on an image corrected FEI Titan Themis).

For SEM investigation a LYRA3 (Tescan Orsay holdings, Brno - Kohoutovice, Czech Republic) SEM was used.

# Determination of the coefficient of thermal expansion (CTE)

For CTE measurements a Dilatometer 402 C (Netzsch, Germany) was used with samples 25x3x1 mm in geometry. Experiments were conducted under controlled Ar atmosphere.

# Thermal cycling procedure

For the thermally cycled TBC samples ERBO 1 substrates were used. The single crystal superalloy ERBO 1 (composition see Table 2) investigated within the SFB-Transregio 103, was casted by the service project Z01 of the SFB-Transregio 103. The service project is allocated at Friedrich-Alexander Universität Erlangen-Nürnberg. Substrate material was cut into 3 mm plates with 30 mm diameter by spark erosion. Edges of the samples were rounded by machining and the surface was cleaned by grit blasting, resulting in a constant substrate roughness of  $2.73\pm0.22~\mu m$   $R_a$ .

For performance analysis of the TBC systems all samples were thermally cycled until failure of the coating occurred. The definition of the coating failure was at least 5 mm coating delamination and/or loss of the heat protection function, indicated by significant deviation in the sample surface temperature (like in [5]). The surface of the samples was heated by a natural gas/oxygen flame, while the backside was cooled by pressurized air, which creates a thermal gradient within the coating. The surface temperature on a spot size of 12 mm was measured by pyrometry (K1SII ,Heitronics, Wiesbaden, Germany) operating at 8-13  $\mu$ m and was adjusted to 1400°C, while the substrate temperature, measured by thermocouple, was kept constant at 1050 or 1080°C. For pyrometry the emissivity was assumed as  $\epsilon$ =1 which results in slightly underestimated temperatures. Every 5 minutes the surface heating was automatically interrupted by pressurized air cooling for 2 minutes. Assuming homogeneous one dimensional thermal conductivities of the layers, the bond coat temperature was calculated by the use of the sample layer thicknesses,

substrate- and surface-temperatures [22]. The top coat thermal conductivity was assumed as 1 W/(mK), which already considers to some degree an increase of thermal conductivity of the top coat due to aging at high temperatures [23]. The bond coat's and the substrate's thermal conductivity was assumed as 31 W/(mK) and 26 W/(mK) for the standard (non ODS) bond coat, respectively. All sample data are presented in Table 4.

# Thermal conductivity

The thermal diffusivity of the ODS was measured by laser flash analysis on 10 mm diameter and 1 mm thick free standing ODS bond coats using a Nd-YAG-Laser with a pulse length of 0.1 to 2 ms in an LFA 427 (Netzsch, Germany) under Helium atmosphere at 0.1 Pa. The heat capacity was measured from 40-1200°C in 5°C steps for 0 and 30 % alumina ODS by a DSC 404 F1 Pegasus (Netzsch, Germany) and was assumed to increase linearly with increasing Al content to allow the calculation of all thermal conductivities. To extract the thermal capacity for the temperature values needed for the thermal conductivity calculation the thermal capacity was averaged over 5 values around the needed temperature. The density of the ODS material was measured at room temperature by geometry and weight of the LFA samples. Densities at high temperatures were calculated using the measured linear thermal expansion coefficients. The thermal conductivity was calculated using thermal diffusivity, thermal capacity and density at different temperatures.

## Thermal cycling sample preparation

The TBC sample cross sections were polished, platinum sputtered and analysed by electron microscope using a Phenom (Phenomworld B.V., Eindhoven, Netherlands and a Hitachi TM3000 (Hitachi High-Technologies Europe GmbH, Krefeld, Germany). The optical analysis was performed by a laser-scanning microscope Keyence VK-9710 (Neu-Isenburg, Germany). Layer

thicknesses were determined by thickness average out of multiple SEM/laser microscope images (top coat, beta depletion thickness 5 laser images; TGO, bond coat, ODS bond coat thickness 10 SEM images). For each image the layer thicknesses were measured by AnalySIS (Olympus Soft imaging solutions GmbH) software with 20 measurements per image. The thickness errors correspond to the standard deviation of the mean values for each image. Top coat porosities were evaluated through the contrast between pores and bulk material in SEM images by the use of several images and AnalySIS imaging software. The error given for the sample porosity values is the standard deviation of the porosity values of 10 images. The ODS alumina content in vol. % was calculated with 3.98 g/cm³ for bulk alumina and 7.47 g/cm³ for CoNiCrAlY bulk material. All data of non-ODS and 2 % TBC samples were taken from [5] and the BC temperature was recalculated with the measured BC thermal conductivities.

Table 3 Process parameters for thermal spray

System	Plasma	Current	Voltage	Ar/H	Feeding	Powder	Pressure	Distance	Robot
	Torch	[A]	[V]	[slpm]	Gas Ar	feeder		[mm]	Speed
					[slpm]				[mm/s]
VPS	F4	640	70	50/9	1.7	15 %	60 mbar	275	440
		/680							
		(ODS)							
APS	Triplex	420	90	46/0	2	20 %	1 atm	200	500
	Pro								
	$210_{TM}$								

## Results and discussion

The major aim of this study is the investigation of the influence of the alumina content in ODS bond coat materials on the oxidation behaviour. Firstly, the oxidation behaviour is discussed by elucidating the influence of the ODS content and the surface state (polished or as-sprayed). Secondly the performance of the ODS bond coat material in a YSZ TBC system is evaluated.

# Oxidation of high alumina content ODS material

Figure 1 shows the specific mass gain over time of the free standing ODS bond coat samples.

According to the total mass gains (polished) two general results are noteworthy:

Firstly, it can be generally stated that all ODS samples show enhanced oxidation resistance (i.e., lower mass gain) compared to non-ODS material. This is in line with previous studies, which already revealed a higher oxidation resistance for polished 2 % ODS bond coat material in comparison to non-ODS material [18].

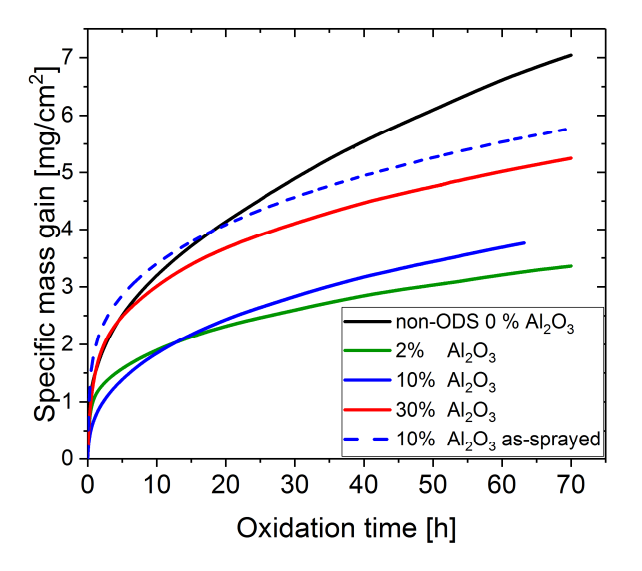


Fig. 1 Thermogravimetric results for polished and as-sprayed ODS bond coat material with different alumina contents oxidized for 0-70 h (63 h for 10 % polished) at 20 % oxygen 80 % argon atmosphere at 1100°C

Secondly, all as-sprayed samples show significantly increased mass gain compared to the corresponding polished samples, as it is exemplarily visualized for the 10 % ODS sample.

Among all polished ODS samples the 2 % material has the lowest final mass gain, followed by the 10 and 30 % ODS samples. Whereas an addition of 30 % alumina leads to an unambiguous decrease of the oxidation resistance and 10 % ODS material indicates only a marginally increased final mass gain compared to 2 % ODS material. However, for early stages of oxidation, it is

worth noting that 10 % ODS material shows a slower oxidation rate compared to 2 % ODS material.

The alumina scale thicknesses presented in Figure 2 qualitatively fit to the total mass gains presented in Figure 1. However, knowing that the RE enrichment in the oxide scale is influenced by the alumina additions in the BC [5,9,17,18], and the high alumina addition (Figure 3) certainly influences the transport mechanisms in the alloy, the thickness of the alumina scale cannot be seen as a decisive quantity for its protectiveness. Since at later stages of oxidation the inward diffusion of oxygen through protective alumina scale is the rate limiting factor of the oxidation kinetics, a more detailed look on the reactive element effect (RE-effect) and "RE over doping", as well as the interplay of ODS particles and the metallic Y-containing matrix shall be taken. The requirement for an enhanced oxidation resistance due to RE addition is a certain concentration of reactive elements within the oxide scale during oxide growth. Delaunay et al. describe an optimum RE (yttrium) concentration in the alloy to be at about 100-300 ppm for a FeNiCrAl system [6]. If a too small amount of yttrium is present, the effect is beneficial but not fully developed. On the other hand, if a too high amount of yttrium is present, "over doping" of the TGO occurs, causing RE rich precipitates such as Y<sub>3</sub>Al<sub>5</sub>O<sub>12</sub> or YAlO<sub>3</sub> to nucleate. These aluminates are believed to enhance inward oxygen diffusion either through the particle itself or via the interphase between the particle and the surrounding alumina. This enhanced inward oxygen diffusion results in an increased oxidation rate [18,24–27], meaning that RE addition is not solely beneficial, as the effect depends on the RE content and hence on the operative

In the literature, the higher oxidation resistance of a 2 % ODS material is related to the suppression of this RE "overdoping" and consequently to the prevention of yttrium aluminate

mechanism.

formation [9] [18]. Since RE-oxides are thermodynamically more stable than alumina, REs are able to reduce aluminum oxide via a solid state reaction. For yttrium reaction (1) can take place.

$$Al_2 O_3 + 2Y \to Y_2 O_3 + 2Al$$
 (1)

Based on reaction (1), alumina particles in the ODS bond coats can act as reaction spots for metallic REs and by that lower their concentration in the alloy and simultaneously increase the Al availability [17,18]. The solid state reaction is diffusion based and is thus expected to be relatively slow, implying that it can solely marginally proceed during manufacture, since the spray process is too short. This means that reaction (1) will restart during high temperature oxidation. Due to the progression of reaction (1) the Y availability within the alloy gets reduced during exposure and the formation of yttrium-aluminates in the oxide scale can be hindered. Accordingly, a lower mass gain of ODS samples in comparison to non-ODS material has been observed because without Y aluminates in the TGO less oxygen pathways through the alumina scale are available [5,9,17,18]. Y-aluminates are visible in the oxide scale of the non-ODS material as bright areas marked by arrows (see Figure 4). Furthermore, at those points where RE-aluminates are located, the TGO shows a distinctive thickness increase.

Both findings indicate an increased Y content in the non-ODS material and an amplified oxygen transport through the scale near RE-aluminates [24], leading to the comparably poor oxidation resistance of the non-ODS material. Furthermore, the lack of those precipitates in the case of the 2 % ODS samples reveals a lowered Y concentration.

10 and 30 % ODS material possess a higher alumina amount in the bond coat in comparison to the 2 % ODS material (see ODS volume fraction presented in Figure 3). Based on a higher alumina volume fraction, a lower amount of Y is expected to remain in the bond coat matrix and an insufficient RE effect is expected to originate. This low amount of remaining Y seems to be one reason for 30 % alumina ODS materials showing a reduced oxidation resistance in

comparison to 2, 10 % ODS. In other words, the Y enrichment within the TGO is expected to be closer to optimum for the 2 and 10 % ODS than for the 30 % sample, resulting in thin and well protecting alumina scales. For the 30 % ODS sample, a too low and for the 0 % a too high amount of Y is present in the TGO.

The following TEM investigations of the scales provide a closer look on the Y availability. The images and element mappings of the oxide scale, presented in Figure 5 reveal yttrium within the alumina scale for 2, 10 and 30 % ODS material. For the 2 and 10 % ODS samples, an yttrium enrichment at the grain boundaries can be clearly identified. For the 30 % sample, an enrichment is present but seems to be less pronounced than for 2 and 10 % ODS oxide scales.

This less pronounced enrichment might appear due to the reduced yttrium availability in the 30 % ODS material in combination with a much smaller alumina scale grain size within the TGO (Figure 6). As a consequence of the smaller grain size, a higher demand of yttrium is needed to reach the optimal concentration at the scale grain boundaries for a pronounced RE effect. Additionally, the Y availability according to reaction (1) is low, due to the high amount of alumina in the 30 % ODS material. As a result of this "limited" Y enrichment, the 30 % ODS sample shows a thick but less protective alumina scale in comparison to 2 and 10 % ODS material.

Apart from the final oxidation resistance a reason for the different ranking of oxidation resistance in the early stage of oxidation shall be mentioned.

Firstly, at the early stage of oxidation spinel formation influences the oxidation resistance (see bright outer layer in Figure 4). This spinel formation contributes to the comparably pronounced mass gain for the 30% ODS sample. A possible mechanism is that spinel formation occurs at high oxygen partial pressures until the spinel reduces the oxygen partial pressure at the metal scale

partial pressures. The microstructure of the 30 % alumina ODS material might have an influence on the spinel microstructure. As visible in Figure 4 the spinel layer is highly porous. Therefore the spinel forming on 30 % ODS material seems to allow enhanced oxygen diffusion leading to a thick spinel layer until the oxygen partial pressure at the metal scale interface is reduced below the stability limit of the spinel. According to Figure 5, the spinel layer consists mainly of Co and Cr oxides.

Secondly, the mass gain of the 2 % ODS material initially exceeds the mass gain of 10 % ODS material resulting in a different order of oxidation resistances than after 70 h (63 h) of exposure. A link for this behavior might be the formation of a porous Cr-containing (see Figure 5) upper part of the alumina TGO, see Figure 4, which is much more pronounced for the 2 % ODS sample than for the 10 % ODS sample. According to Unocic et al. [9] and Pint et al. [12] the formation of this layer can be ascribed to initial oxide formation. Due to the high porosity its growth might go along with accelerated oxidation kinetics comparable to a dense oxide scale leading to a different oxidation resistances of 2 and 10 % ODS material in the first hours of oxidation. Another reason for the mass gain of the 2 % ODS material initially exceeding the mass gain of 10 %ODS material might be the higher reactive surface fraction (Figure 3) of 2 % ODS material in comparison to the 10 % ODS material. 30 % ODS material has a lower surface fraction and from this point of view should have the lowest mass gain at the early stage of oxidation but the 30 % ODS material is highly affected by spinel formation which - as mentioned above - leads to the high mass gains in the first hours of oxidation.

Besides ODS content-derived influences among the polished samples, additionally the surface state (polished or as-sprayed) was determined as an important factor of impact. Since in a TBC

system under thermal exposure the oxide scale forms on the as-sprayed bond coat surface and not on a polished one, these results are especially interesting [28–31]. It needs to be mentioned that the as-sprayed samples used for isothermal oxidation experiments underwent no vacuum annealing and preheating and hence are slightly different from those discussed in the course of the TBC performance analyses.

All as-sprayed samples showed a decreased oxidation resistance compared to the correspondent polished samples. An example for a higher mass gain the data of the 10 % ODS sample in as sprayed state was exemplary added to Figure 1.

Since the as-sprayed sample exhibits one spark-eroded side, mass gain differences among the assprayed samples will not be quantitatively discussed in the course of this work. One reason for the enhanced oxidation kinetics of the as sprayed samples is the higher surface roughness offering a higher surface area on the as-sprayed surfaces compared to the polished surfaces.

For the 0 % ODS sample, it is furthermore noteworthy that in the as-sprayed state, an accumulation of aluminates within the valleys of the alloy/TGO-interface is present. Since a higher roughness fosters the yttrium depletion in the bond coat, at the tip of a wavy bond coat the yttrium availability for the growing TGO is lower than in the valley [32]. According to [30], this concentration difference results in an enhanced yttrium aluminate formation in the valleys for the 0 % ODS scale (Figure 4). This effect is visible for 0 % ODS TGA as sprayed sample because of the initial high surface roughness (Figure 7). No aluminates are found in the roughness valleys of 2 % ODS or any of the other ODS as-sprayed samples. This result indicates a strong Y-trap effect of the ODS particles.

Additionally an increased tendency for spinel formation is visible for the as-sprayed 10 % and 30 % ODS samples, what might also cause a deterioration of the oxidation resistance compared to the polished counterparts.

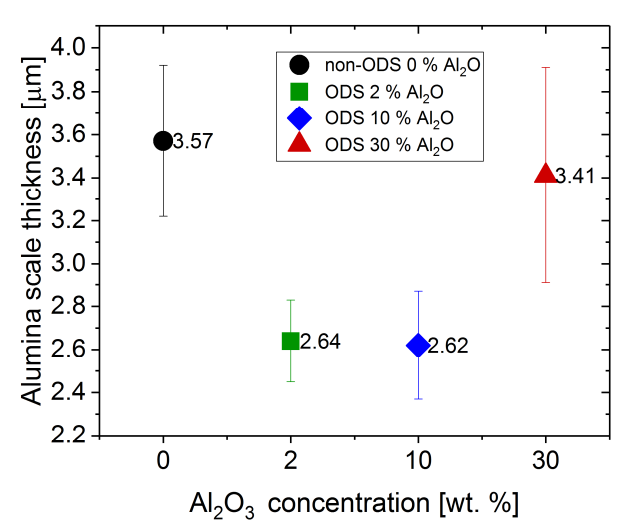


Fig. 2 Alumina scale thickness for polished samples after 70 h (62 h for 2 % alumina) at 1100°C in 20 %  $O_2$  in Ar

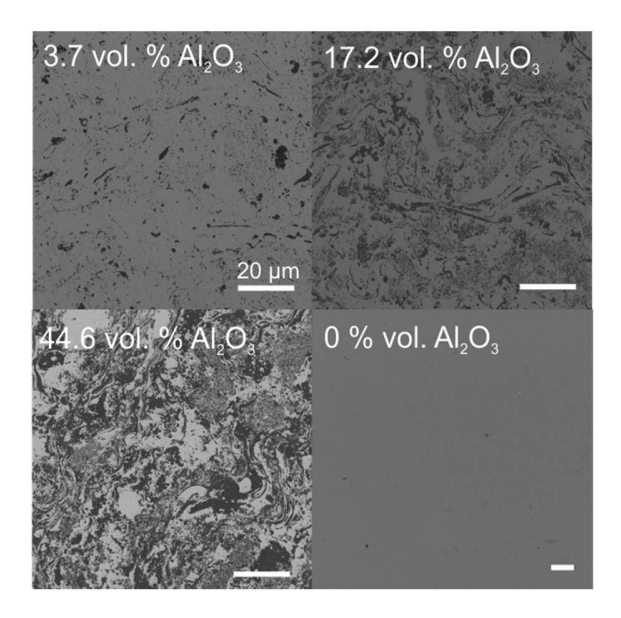
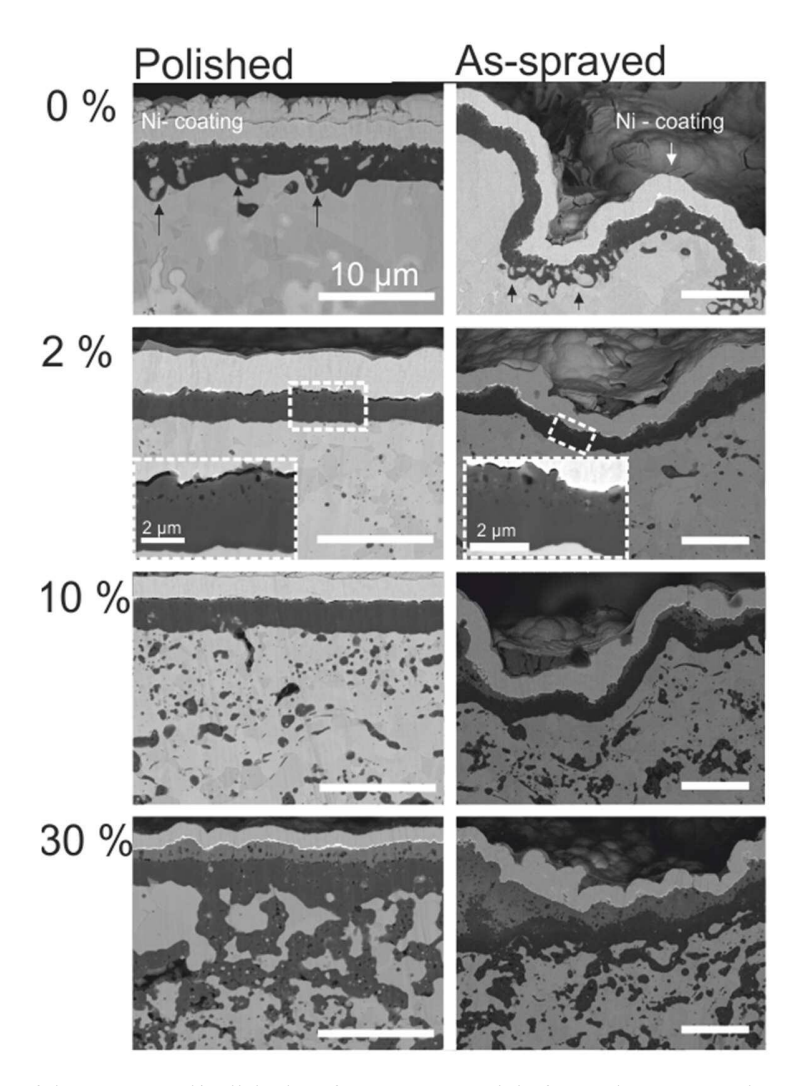


Fig. 3 SEM cross section of thermally sprayed ODS material with different alumina volume fractions (calculated by the weight ratio of alumina and CoNiCrAlY) showing homogeneous alumina embedding in the alloy matrix



**Fig. 4** SEM images of the as-sprayed/polished surface ODS material after 70 h at 1100°C in 20 % oxygen in argon (63 h for 2 % polished) showing yttrium aluminate containing TGO for non ODS- 0 % alumina (marked by the arrows). TGO nearly without yttrium aluminates is visible for 2 % and 10 % alumina ODS bond coat material. A double layered/spinel containing oxide layers are visible for 30 % alumina ODS. A partly porous (Co containing - Fig. 5) alumina layer is visible for 2 % rough surface was analysed with lower magnification due to visibility of roughness

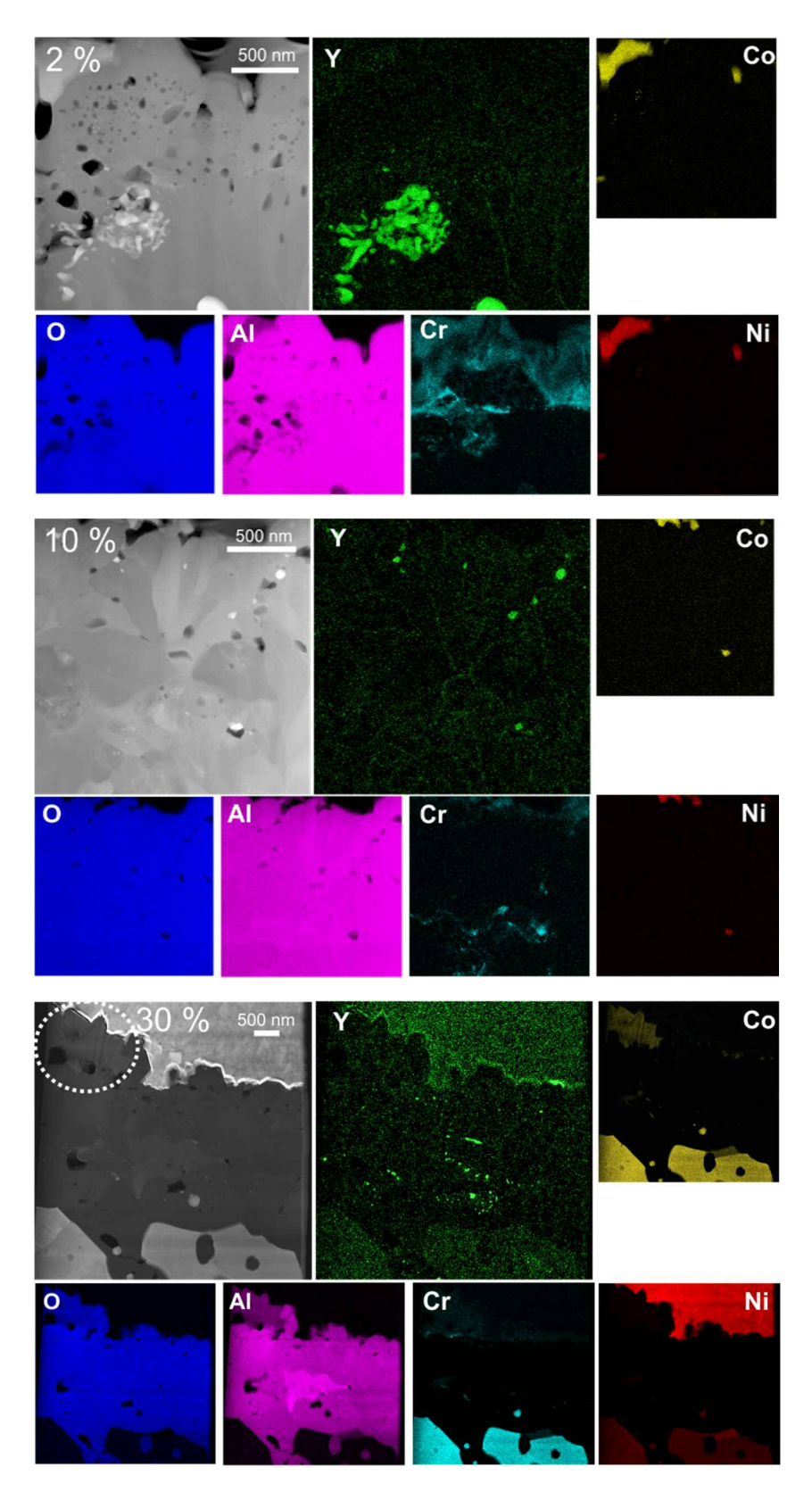


Fig. 5 HAADF Transmission electron microscopy and element mapping of the oxide scale on 2% (70 h), 10% (63 h), and 30% (70 h) alumina ODS material (after  $1100^{\circ}$ C with 20% oxygen in Argon)

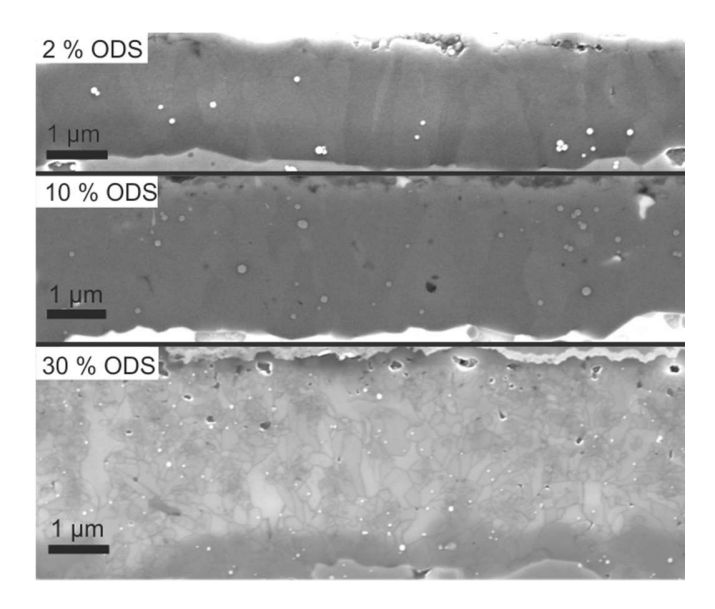


Fig. 6 In Lens SEM images of the oxide scale for 2, 10, and 30 % ODS material after 70 h at 1100°C in 20 % O<sub>2</sub> 80 % Ar showing finer grain size for 30 % ODS and columnar grains for 2 and 10 % ODS material, image contrast was adjusted to grain boundary visibility

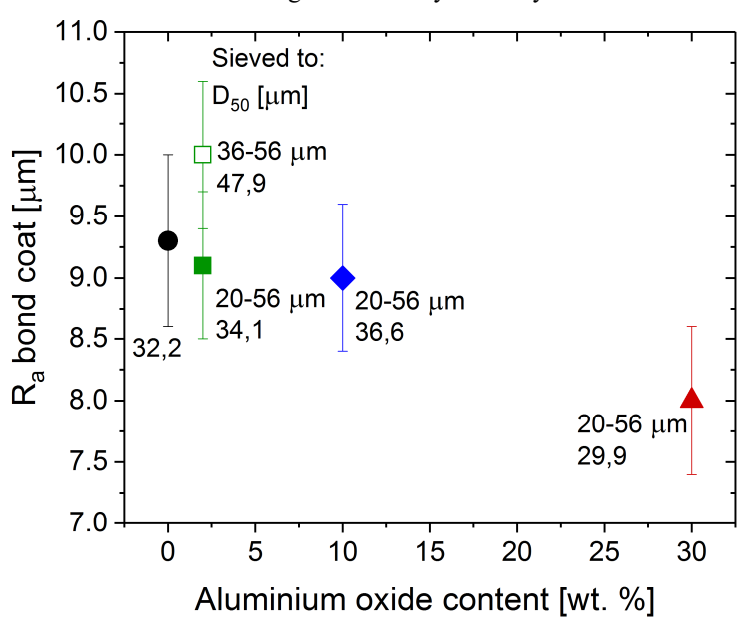


Fig. 7 Surface roughness of vacuum plasma sprayed ODS bond coats with increasing alumina content in relation to the sieving fraction/ $D_{50}$  value of the powder showing decreasing roughness with decreasing  $D_{50}$  values of the ODS powders, slightly different roughness for empty symbol corresponding to the batch of TBC samples of the 2 % ODS

# Thermal Cycling Results

For comparison of the performance of the different bond coats in a complete TBC system, the different bond coats were sprayed on a single crystal superalloy samples and were additionally coated with YSZ top coat. These complete TBC systems were thermally cycled to failure to evaluate the performance of the different bond coats. For an oxidation induced failure through TGO growth, the bond coat temperature under test conditions has a major influence on the thermal cycling performance, due to the temperature influence on the bond coat oxidation [19,33]. For calculation of bond coat temperature, thermal conductivities of each layer are needed [22]. ODS bond coat thermal conductivities at different temperatures were measured. The thermal conductivity in (Figure 8) shows a decreasing thermal conductivity for increasing alumina content in the ODS material. For the temperature under test conditions (about 1000°C) the thermal conductivity of 30 % ODS material is less than half of the non ODS material's thermal conductivity.

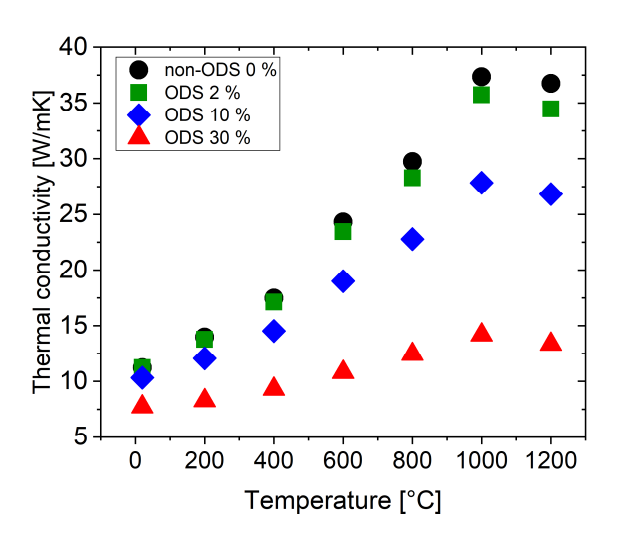


Fig. 8 Thermal conductivity values for bond coats with different aluminum oxide contents at different temperatures showing lower conductivity for higher alumina content

Therefore, thicker ODS bond coats have the advantage that they can provide an additional second thermal protection layer besides the top coat, however also increasing the oxidation temperature of the bond coat. The bond coat temperature under thermal cycling conditions was calculated using the bond coat thermal conductivity at 1000°C.

For comparison of the TBC performance the bond coat temperature is taken into account. Therefore the logarithm of the number of cycles to failure of the TBCs is plotted against the inverse bond coat/ top coat interface temperature (Figure 9).

For an oxidation induced failure, the logarithm of the number of cycles to failure of the TBCs samples is proportional to the inverse bond coat temperature [19,33,34]. This linear scale dependency according to Vaßen et al. [19] is added to the graph. To compare the TBC systems, the linear scale dependency was extrapolated for the performance of TBC systems with non-ODS (0 % ODS), 2 % and 10 % ODS bond coat TBCs. For the 30 % ODS samples this extrapolation is not valid, as explained below.

As reported in a previous study, the performance increase of non-ODS and 2 % ODS TBC systems in comparison to reference TBC systems is related to the lower thermal expansion coefficient of the substrate ERBO1, enhanced oxidation resistance of the 2 % ODS, and enhanced bond coat roughness increasing the top coat adhesion [5]. The data of the TBCs without ODS and 2 % ODS [5] is now used for comparison with higher alumina content ODS TBCs.

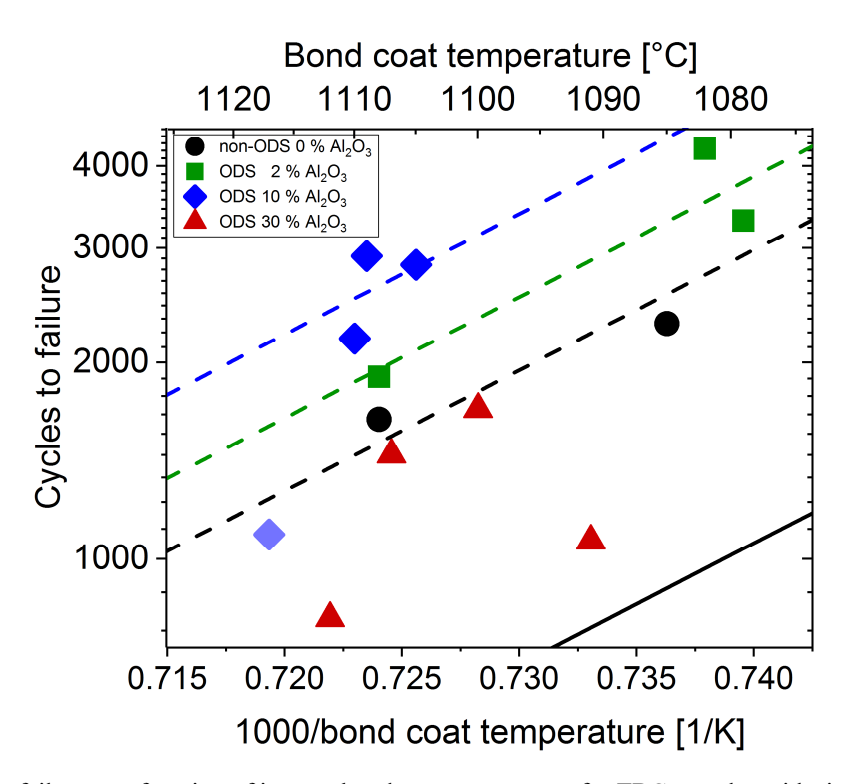


Fig. 9 Cycles to failure as a function of inverse bond coat temperature for TBC samples with single layered or advanced double layered with top oxide dispersion strengthened bond coats with 2, 10, 30 %  $Al_2O_3$  and 500  $\mu m$  porous YSZ top coat on single crystal superalloy ERBO 1 substrates, black line represents linear dependency - equal performance line - with TBC's on IN738 [19], dashed lines marking extrapolated performance lines of different TBC systems

TBCs with higher 10 % alumina content in the ODS bond coat show a further performance increase, while 30 % ODS bond coats result in a lower TBC performance (Figure 9). Several effects lead to this performance behaviour.

The 10 % ODS material has a similar oxidation resistance compared to 2 % ODS (Figure 1) but shows enhanced lifetime. The performance enhancement of 10 % ODS is caused by the reduced CTE mismatch between top coat and ODS bond coat which reduces crack formation at the interface between top coat and bond coat. A detailed view on the failure mechanism of the TBC systems outlines this CTE lifetime relation.

If the TBC system is assumed stress free at high temperatures, the thermal expansion coefficient mismatch of the top coat (CTE YSZ 10-11 10<sup>-6</sup> [1/K] [35]) and the bond coat (CTE 12.7-16.6 10<sup>-1</sup>

<sup>6</sup> [1/K] -Fig. 10) material causes stresses at the weavy interface of the bond coat/ top coat during cooling, which leads to cracks at the tips [32,36–38]. For 10 % ODS material the thermal expansion coefficient is lower in comparison to 2 % ODS (Figure 10), leading to a lower CTE mismatch resulting in less crack formation at the tip of the interface.

Through TGO growth and the very low thermal expansion coefficient of the TGO, a stress field inversion at the valleys of a rough bond coat/ top coat interface occurs in the later stage of oxidation. This stress field inversion leads to crack linking between the cracks initiated through the bond coat/top coat CTE mismatch and lower stress levels. These linking cracks occur in the TGO and within the YSZ and finally can lead to failure of the coating [1,32,39]. In conclusion and comparison to 2 % ODS TBC systems, crack initiation is reduced for 10 % ODS, due to lower CTE mismatch, which, in case of similar oxidation resistance (Figure 1), results delayed crack linking and failure of the TBC. Therefore 10 % ODS TBCs show an enhanced performance compared to 2 % ODS TBCs. Slightly lower roughness of the 10 % ODS bond coat (Figure 7) might reduce the performance enhancement by a lower mechanical clamping of the top coat. Bond coat roughening, also called rumpling, should not occur in case of ODS bond coats. Bond coat rumpling due to thermal cycling depends on the creep and yield strength of the bond coat material and is not affected by the roughness value before thermal cycling [40]. Due to a high creep resistance of the ODS material, bond coat rumpling is not sufficiently pronounced to further modify surface roughnesses of the ODS bond coats and to affect the performance of the TBC systems.

Apart from the high performance of the 10 % ODS bond coat samples, TBCs with 30 % ODS showed a bad thermal cycling performance which is in contrast to the lowest CTE of the 30 % ODS material (Figure 10). Several factors lead to the significant TBC performance decrease of the 30 % ODS TBC samples.

At first glance the poor mechanical porperties of the TGO and the low oxidation resistance might lead to the early failure of the 30 % ODS bond coat samples. An indication is the early failure of the 30 % ODS samples at TGO thicknesses comparable to the other samples (Figure 11). So the above described mechanism of stress inversion might take place much earlier in the 30 % ODS system.

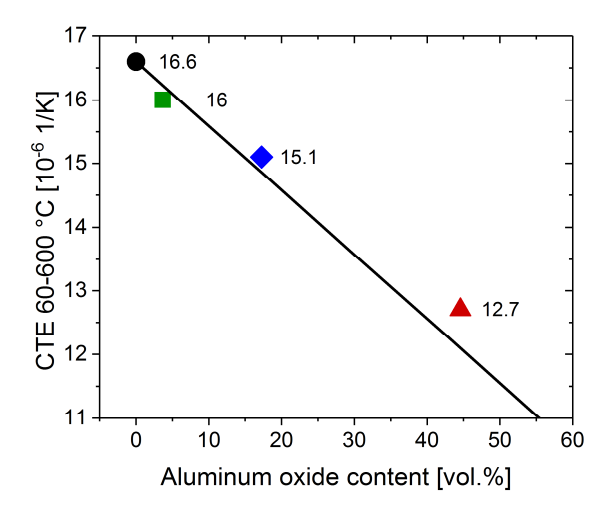


**Fig. 10** Thermal expansion coefficient for oxide dispersion strengthened bond coats with higher alumina content showing a reduced CTE for higher alumina content with slight deviation to the theoretical line extrapolated to the thermal expansion coefficient of alumina.

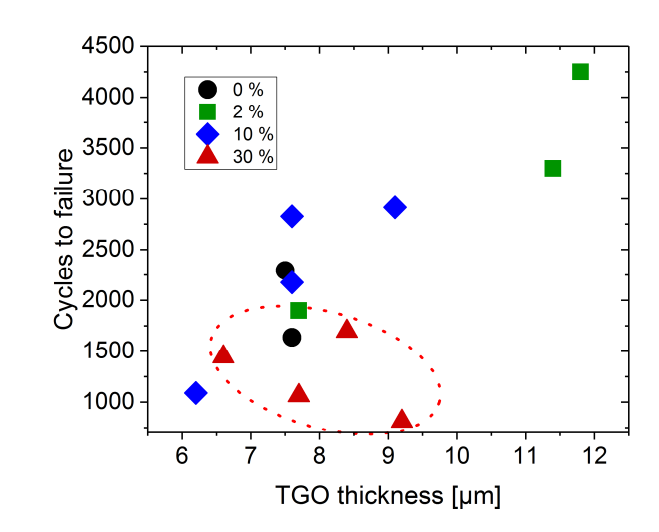


**Fig. 11** Thermally grown oxide thickness (alumina TGO) against cycles to failure for TBC systems using additional thin oxide dispersion strengthened bond coats and standard bond coats showing thick TGO for high number of cycles and similar TGO thicknesses at failure for 30 % ODS bond coats revealing a change in the TGO growth leading to an early failure

However, apart from the bond coat properties the top coat properties have an influence on the TBC failure mode, too. For the 2 and the 10 % ODS the failure of the TBC is close to the bond coat/ TBC-interface both within the TGO or the TBC topcoat (Figure 12), which indicates an oxidation induced failure, so the influence of the top coat should be similar for similar top coat thicknesses (Table 4).

For 30 % ODS, TBCs top coat properties, e.g. fracture toughness, has a significantly higher influence on the lifetime, as the failure of the TBC system shifts in the top coat (Figure 12). Thus extrapolation of the linear temperature scale dependency in the Arrhenius plot for the 30 % ODS is not valid. The low performance of the 30 % ODS bond coat is therefore simply estimated by the low number of cycles to failure of those TBC systems. The failure shift to the top coat might be linked with local high stress levels caused by the massive scale formation of 30 % ODS material in combination with enhanced top coat adhesion supressing cracking at the TGO top coat interface.

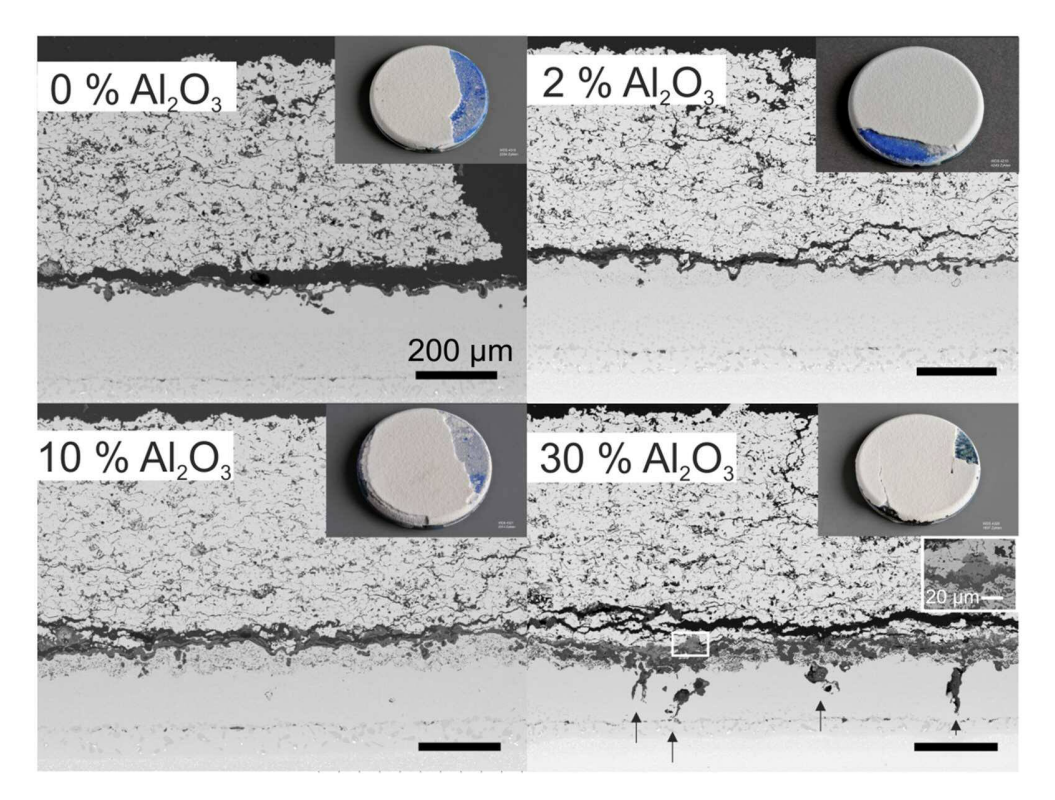


**Fig. 12** TBC cross section and top view for thermally cycled TBCs with non ODS and ODS bond coats with different alumina contents showing a failure within the top coat for higher alumina ODS bond coats, enhanced mechanical clamping of top coat through local spinel formation marked by zoom window, cracks within the bond coat marked by black arrows

Another result during cycling of the 30 % ODS material are cracks within the bond coat, but not within the top ODS bond coat (Figure 12). Cracking of the standard bond coat, only visible for 30 % ODS material, might be related the CTE differences between standard bond coat ( $\alpha$ = 16,6 10<sup>-6</sup> 1/K-), ODS bond coat ( $\alpha$ = 12.7 10<sup>-6</sup> 1/K –) and substrate ( $\alpha$ = 14.6 10<sup>-6</sup> 1/K – at 60-600°C). Assuming a stress free state at room temperature and assuming the thick substrate as the strain affecting layer, the standard bond coat is under compressive stress, as the standard bond coats elongation during temperature increase is blocked by the substrate and additionally by the ODS bond coat. At high temperatures the stresses decrease through e.g. diffusional creep over time. On cooling down the TBC system the standard bond coat is under tensile stress caused by the lower shrinking of both the substrate and the ODS bond coat.

In general the influence of the thin ODS bond coat on the in-plane bond coat stress is marginal as the thick (3 mm) substrate dictates the stress evolution. At the edges additional effects might occur, however, cracks (see Figure 12) are also present in the middle of the samples. As discussed earlier for the TBC failure, also the local curvature and composition at the interface can lead to additional stresses. Assuming a stress free state at elevated temperature (due to diffusional creep processes) the bond coat is under tensile stress at reduced temperatures, due to the lower contraction of the substrate (CTE substrate 14.8 10-6 1/K [5], BC 16.6 10-6 at 60-600°C). At a valley location of the bond coat/ ODS bond coat interface the contraction of the bond coat is further constraint by the low thermal expansion coefficient of the ODS bond coat leading to additional tensile stress in the bond coat. In combination with a kind of notch effect at the valley location this might lead to the observed cracks in the bond coat underneath the ODS bond coat.

In this study it was tried to keep the influence of the topcoat porosity level as low as possible by using constant process conditions. In general, the top coat porosity influences the lifetime of the TBC system, due to different energy release rates in the coating. If the coating is assumed stress free at room temperature, the top coat is under tensile stress due to the larger substrate expansion. At high temperatures these stresses relax e.g. through diffusional creep processes, so after cooling the top coat is under compressive stress leading to a certan energy release rate of the TBC. If this exceeds the critical energy release reate of the system cracks will propagate. The energy release rate in the top coat depends on the Young's modulus and is therefore linked with the porosity of the coating [1,41].

Top coat manufacturing parameters were kept constant resulting in a low variation of the top coat porosity. After thermal cycling all samples show top coat porosities with a variation below 20 % (average of 15.1±2.7 % - Figure 13). The porosity of an uncycled reference sample is slightly

higher at 15.5±1.7 %. Although the porosity changes are small, thre can be major influences of sintering on the performance as in the first stages of sintering by surface diffusion considerable changes of Young's modulus occur without porosity decrease. Sintering effects of the 2 % ODS with very high number of cycles to failure are visble as described in [5].

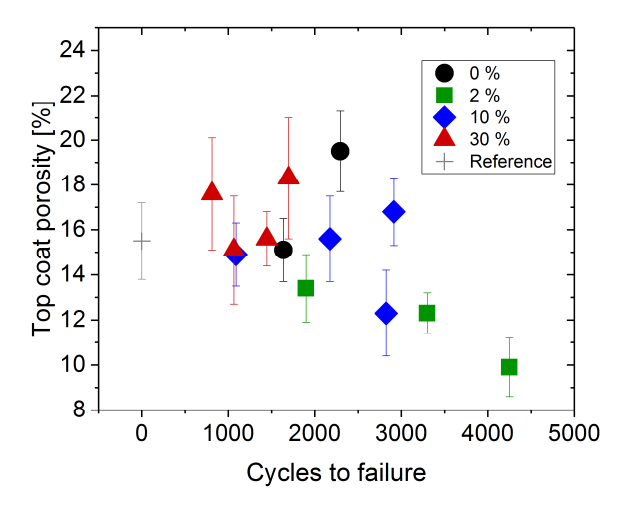


Fig. 13 Top coat porosity against cycles to failure for YSZ TBC systems using additional thin oxide dispersion strengthened bond coats and standard bond coats showing YSZ porosities from 10 to 19 %

A further reason leading to failure of TBC systems are fully depleted bond coats [34]. Through the TGO growth the aluminum reservoir in the bond coat, that is mainly stored in the Al- rich beta phase (Ni Al- Phase), is used. If the bond coat is fully/ too much depleted, the growth of an alumina TGO is no longer possible and spinel formation starts. Through the additional stresses at the top coat/ bond coat interface caused by the spinel formation, an accelerated failure of the coating is fostered.

In case of the TBC systems of the present study, the  $\sim$ 200  $\mu$ m bond coats are not yet fully depleted (Figure 14) - therefore a chemical failure is not expected, even though some spinels are visible for as-sprayed 2 and 10 % ODS samples and more spinels for 30 % ODS.

It is further visible that the ODS bond coats show similar or larger beta (-Ni-Al phase) depletionzone thicknesses, while showing similar TGO thicknesses compared to the non ODS samples (Figure 14). Hence, the beta depletion of ODS samples was measured starting at the

ODS/ non ODS interface the ODS bond coats do not provide as high amount of aluminium as the standard bond coat does.

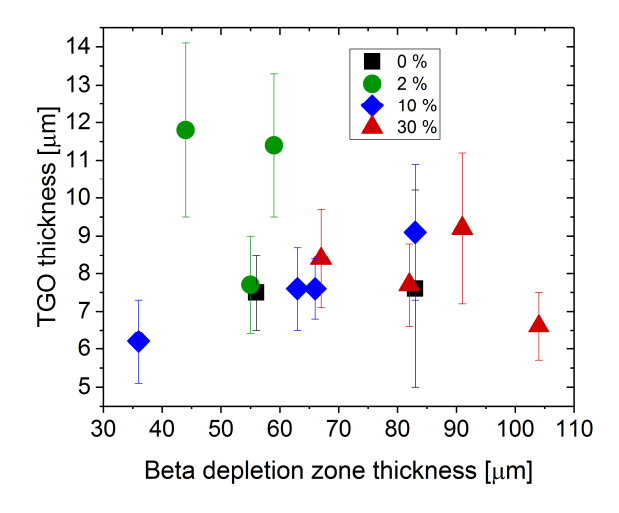


**Fig. 14** Thermally grown oxide (alumina TGO) thickness against the beta depletion zone measured in the standard bond coat for TBC systems using additional thin oxide dispersion strengthened bond coats, the same depletion is visible for standard bond coat and ODS bond coat systems showing a low aluminum reservoir of the ODS bond coat

## **Conclusions**

Aluminum oxide dispersion strenghtened bond coat materials were produced with 2, 10 and 30 % alumina content in a CoNiCrAIY matrix to improve the oxidation behaviour and reduce the thermal expansion coefficient missmatch between top coat and bond coat in a thermal barrier coating system. Low pressure plasma sprayed free standing coatings were analysed regarding their oxidation behaviour. Higher alumina content in oxide dispersion strengthened bond coat materials significantly influences the oxidation resistance of the plasma sprayed material by affecting the Y ion concentration at the alumina scale grain boundaries and supressing the Y overdoping effect. The advanced materials were applied as an additional oxide dispersion strengthened bond coat in thermal barrier coatings. Thermal cycling under conditions close to

operational reveals the oxidation behaviour and the thermal expansion coefficient of the ODS bond coats as major factors affecting the TBC performance. The performance of TBC systems were evaluated by the number of cycles to failure taking into account the bond coat temperature. Effects of top coat sintering and bond coat depletion on the thermal cycling performance were similar for all investigated systems.

The summarized results are:

- Comparable enhanced oxidation resistance is found for 10 % and 2 % alumina ODS materials due to Y-aluminate free TGO no overdoping and at the same time with sufficient presence of Y ions at the alumina scale grain boundaries to reduced oxygen diffusion through the scale.
- 30 % ODS alumina content results in lower oxidation resistance due to enhanced spinel formation and a reduced Y ion concentration in the alumina through enhanced reaction of the alumina in the ODS with the Y of the alloy.
- Faster oxidation kinetics of as-sprayed samples due to higher surface area and enhanced spinel formation as compared to polished samples.
- Superior thermal cycling performance of 10 % alumina ODS due to enhanced oxidation resistance and reduction of the thermal expansion coefficient missmatch between top coat and bond coat.

- Lower thermal cycling performance of 30 % ODS material due to worse oxidation behaviour with massive spinel formation, although 30 % ODS bond coats show a low thermal expansion coefficient adjusted to the YSZ topcoat.

Based on our findings on the oxidation behaviour and thermal cycling results, further investigations would be advisable with 30 % ODS bond coats and increased Y content, to preserve the effect of RE doping and take advantage from the low CTE of the 30 % ODS.

## References

- [1] C. Nordhorn, R. Mücke, D.E. Mack, R. Vaßen, Probabilistic lifetime model for atmospherically plasma sprayed thermal barrier coating systems, Mechanics of Materials 93 (2016) 199–208.
- [2] M. Martena, D. Botto, P. Fino, S. Sabbadini, M.M. Gola, C. Badini, Modelling of TBC system failure, Engineering Failure Analysis 13 (2006) 409–426.
- [3] A.G. Evans, D.R. Mumm, J.W. Hutchinson, G.H. Meier, F.S. Pettit, Mechanisms controlling the durability of thermal barrier coatings, Progress in Materials Science 46 (2001) 505–553.
- [4] B.A. Pint, A.J. Garratt-Reed, L.W. Hobbs, The reactive element effect in commercial ODS FeCrAl alloys, Materials at High Temperatures 13 (1995) 3–16.
- [5] C. Vorkötter, D.E. Mack, O. Guillon, R. Vaßen, Superior cyclic life of thermal barrier coatings with advanced bond coats on single-crystal superalloys, Surface and Coatings Technology 361 (2019) 150–158.
- [6] D. Delaunay, A.M. Huntz, Mechanisms of adherence of alumina scale developed during high-temperature oxidation of Fe-Ni-Cr-Al-Y alloys, J Mater Sci 17 (1982) 2027–2036.
- [7] B.A. Pint, A.J. Garratt-Reed, L.W. Hobbs, Possible Role of the Oxygen Potential Gradient in Enhancing Diffusion of Foreign Ions on  $\alpha$ -Al2O3 Grain Boundaries, Journal of the American Ceramic Society 81 (1998) 305–314.
- [8] B.A. Pint, K.L. More, I.G. Wright, The use of two reactive elements to optimize oxidation performance of alumina-forming alloys, Materials at High Temperatures 20 (2003) 375–386.
- [9] K.A. Unocic, J. Bergholz, T. Huang, D. Naumenko, B.A. Pint, R. Vaßen, W.J. Quadakkers, Hightemperature behavior of oxide dispersion strengthening CoNiCrAlY, Materials at High Temperatures 35 (2017) 108–119.
- [10] D.P. Whittle, J. Stringer, Improvements in high temperature oxidation resistance by additions of reactive elements or oxide dispersions, Phil. Trans. R. Soc. Lond. A 295 (1980) 309–329.
- [11] B. A. Pint (Ed.), Progress in understanding the reactive element effect since the Whittle and Stringer literature review, ASM International Materials Park, Ohio, 2003.

- [12] B.A. Pint, K.L. More, I.G. Wright, P.F. Tortorelli, Characterization of thermally cycled alumina scales, Materials at High Temperatures 17 (2000) 165–171.
- [13] B.A. Pint, Experimental observations in support of the dynamic-segregation theory to explain the reactive-element effect, Oxid Met 45 (1996) 1–37.
- [14] A. Gil, D. Naumenko, R. Vassen, J. Toscano, M. Subanovic, L. Singheiser, W.J. Quadakkers, Y-rich oxide distribution in plasma sprayed MCrAlY-coatings studied by SEM with a cathodoluminescence detector and Raman spectroscopy, Surface and Coatings Technology 204 (2009) 531–538.
- [15] E. Hejrani, D. Sebold, W.J. Nowak, G. Mauer, D. Naumenko, R. Vaßen, W.J. Quadakkers, Isothermal and cyclic oxidation behavior of free standing MCrAlY coatings manufactured by high-velocity atmospheric plasma spraying, Surface and Coatings Technology 313 (2017) 191–201.
- [16] J. Toscano, R. Vaβen, A. Gil, M. Subanovic, D. Naumenko, L. Singheiser, W.J. Quadakkers, Parameters affecting TGO growth and adherence on MCrAlY-bond coats for TBC's, Surface and Coatings Technology 201 (2006) 3906–3910.
- [17] Jan Bergholz, Herstellung und Charakterisierung oxiddispersionsverstärkter Haftvermittlerschichten. Dissertation, 2016.
- [18] T. Huang, J. Bergholz, G. Mauer, R. Vassen, D. Naumenko, W.J. Quadakkers, Effect of test atmosphere composition on high-temperature oxidation behaviour of CoNiCrAlY coatings produced from conventional and ODS powders, Materials at High Temperatures 2 (2018) 97–107.
- [19] R. Vaßen, S. Giesen, D. Stöver, Lifetime of Plasma-Sprayed Thermal Barrier Coatings, J Therm Spray Tech 18 (2009) 835–845.
- [20] J. Bergholz, B.A. Pint, K.A. Unocic, R. Vaßen, Fabrication of Oxide Dispersion Strengthened Bond Coats with Low Al2O3 Content, J Therm Spray Tech 26 (2017) 868–879.
- [21] Philipp J. Terberger, Alterung von Vakuum-plasmagespritzten MCrAlY-Schutzschichten und ihre Wechselwirkung mit Nickel- und Cobalt y-y' mbasierten Superlegierungen. Dissertation, 2015.
- [22] F. Traeger, R. Vaßen, K.-H. Rauwald, D. Stöver, Thermal Cycling Setup for Testing Thermal Barrier Coatings, Adv. Eng. Mater. 5 (2003) 429–432.
- [23] H.-J. Rätzer-Scheibe, U. Schulz, The effects of heat treatment and gas atmosphere on the thermal conductivity of APS and EB-PVD PYSZ thermal barrier coatings, Surface and Coatings Technology 201 (2007) 7880–7888.
- [24] B.A. Pint, Optimization of Reactive-Element Additions to Improve Oxidation Performance of Alumina-Forming Alloys, J American Ceramic Society 86 (2003) 686–695.
- [25] D. Naumenko, J. Le-Coze, E. Wessel, W. Fischer, W. Quadakkers, Joseph, Effect of Trace Amounts of Carbon and Nitrogen on the High Temperature Oxidation Resistance of High Purity FeCrAl Alloys, Mater. Trans. 43 (2002) 168–172.
- [26] T.A. Ramanarayanan, The Characteristics of Alumina Scales Formed on Fe-Based Yttria-Dispersed Alloys, J. Electrochem. Soc. 131 (1984) 923.
- [27] M. Subanovic, D. Sebold, R. Vassen, E. Wessel, D. Naumenko, L. Singheiser, W.J. Quadakkers, Effect of manufacturing related parameters on oxidation properties of MCrAlY-bondcoats, Materials and Corrosion 59 (2008) 463–470.
- [28] F. Naeimi, M.R. Rahimipour, M. Salehi, Effect of Sandblasting Process on the Oxidation Behavior of HVOF MCrAlY Coatings, Oxid Met 86 (2016) 59–73.

- [29] A. Gil, V. Shemet, R. Vassen, M. Subanovic, J. Toscano, D. Naumenko, L. Singheiser, W.J. Quadakkers, Effect of surface condition on the oxidation behaviour of MCrAlY coatings, Surface and Coatings Technology 201 (2006) 3824–3828.
- [30] F. Tang, L. Ajdelsztajn, G.E. Kim, V. Provenzano, J.M. Schoenung, Effects of surface oxidation during HVOF processing on the primary stage oxidation of a CoNiCrAlY coating, Surface and Coatings Technology 185 (2004) 228–233.
- [31] N. Czech, M. Juez-Lorenzo, V. Kolarik, W. Stamm, Influence of the surface roughness on the oxide scale formation on MCrAlY coatings studied in situ by high temperature X-ray diffraction, Surface and Coatings Technology 108-109 (1998) 36–42.
- [32] D. Naumenko, V. Shemet, L. Singheiser, W.J. Quadakkers, Failure mechanisms of thermal barrier coatings on MCrAlY-type bondcoats associated with the formation of the thermally grown oxide, J Mater Sci 44 (2009) 1687–1703.
- [33] F. Traeger, M. Ahrens, R. Vaßen, D. Stöver, A life time model for ceramic thermal barrier coatings, Materials Science and Engineering: A 358 (2003) 255–265.
- [34] S. Rezanka, G. Mauer, R. Vaßen, Improved Thermal Cycling Durability of Thermal Barrier Coatings Manufactured by PS-PVD, J Therm Spray Tech 23 (2014) 182–189.
- [35] R. Vaßen, F. Traeger, D. Stöver, New Thermal Barrier Coatings Based on Pyrochlore/YSZ Double-Layer Systems, International Journal of Applied Ceramic Technology 1 (2004) 351–361.
- [36] N.P. Padture, M. Gell, E.H. Jordan, Thermal barrier coatings for gas-turbine engine applications, Science (New York, N.Y.) 296 (2002) 280–284.
- [37] W. Nowak, D. Naumenko, G. Mor, F. Mor, D.E. Mack, R. Vassen, L. Singheiser, W.J. Quadakkers, Effect of processing parameters on MCrAlY bondcoat roughness and lifetime of APS–TBC systems, Surface and Coatings Technology 260 (2014) 82–89.
- [38] K. Schlichting, N. Padture, E. Jordan, M. Gell, Failure modes in plasma-sprayed thermal barrier coatings, Materials Science and Engineering: A 342 (2003) 120–130.
- [39] C. Nordhorn, R. Mücke, R. Vaßen, Simulation of the effect of realistic surface textures on thermally induced topcoat stress fields by two-dimensional interface functions, Surface and Coatings Technology 258 (2014) 181–188.
- [40] V.K. Tolpygo, D.R. Clarke, On the rumpling mechanism in nickel-aluminide coatings, Acta Materialia 52 (2004) 5115–5127.
- [41] J.F. Knott, Fundamentals of fracture mechanics, Pe Men Book Co, Taipei, 1981.

Table 4 Specifications of samples after thermal cycling

Sample (internal number)	Cycles to failure	TGO thickness [µm]	ODS bond coat thickness [µm]	Beta depletion zone thickness [µm]	Standard bond coat thickness [µm]	R <sub>a</sub> bond coat [μm]	Bond coat temperature [°C]	Top coat porosity [%]	Top coat thickness [µm]
0 % I (4310)	2294	7.5±1.0	n.a.	56±3	238±4	9.4	1085	19.5±1.8	511±6
0 % II (4309)	1637	7.6±2.6	n.a.	83±7	170±8	9.4	1108	15.1±1.4	578±6
2 % I (4214)	3300	11.4±1.9	44±4	59±9	126±6	9.9	1076	12.3±0.9	533±8
2 % II (4215)	4249	11.8±2.1	43±4	44±9	162±4	10.2	1082	9.9±1.3	511±6
2 % III (4213)	1899	7.7±1.3	45±6	55±13	147±7	9.9	1108	13.4±1.5	507±12
10 % I (4321)	2914	9.1±1.8	55±5	83±4	130±11	8.9	1109	16.8±1.5	557±11
10 % II (4322)	1089	6.2±1.1	50±5	36±7	143±8	8.8	1117	14.9±1.4	560±7
10 % III (4320)	2176	7.6±0.8	56±9	66±12	149±8	9.0	1110	15.6±1.9	576±4
10 % IV (4319)	2825	7,6±1,1	54±6	63±7	13+±7	9.0	1105	12.3±1.9	581±11
30 % I (4328)	1697	8.4±1.3	44±8	67±18	134±12	8.4	1100	18.3±2.7	551±12
30 % II (4329)	1065	7.7±1.1	46±9	82±11	137±11	7.7	1088	15.1±2.4	566±13
30 % III (4327)	812	9.2±2	54±4	91±27	135±9	9.2	1112	17.6±2.5	556±6
30 % IV (4326)	1445	6.6±0.9	60±8	104±6	135±12	8.0	1107	15.6±2.5	564±9

# **Acknowledgements:**

This work was funded by SFB Transregio 103 (Project number B6). We thank our cooperation partners for the supply of the single crystal superalloy material. A big thanks goes to Dr. Aleksander Kostka and colleagues at MPI Düsseldorf for the high resolution TEM element mappings.

The authors acknowledge the contribution of the following colleagues in our Institute:

Mr. Ralf Laufs, Mr. Frank Kurze and Mr. Karl-Heinz Rauwald for the invaluable assistance during plasma spraying and Mr. Martin Tandler for the effort with the cyclic burner rig tests. We also would like to thank Dr. Doris Sebold for SEM analysis and assistance and our colleagues at ZEA-3, Forschungszentrum Jülich, Germany, who performed the chemical analysis.

Further thanks goes to Mr. Friedel Gormann who performed the thermal capacity and diffusivity measurements, as well as to Marie-Theres Gerhards for the thermal expansion coefficient measurements.